



HAL
open science

The role of fluorine in high quantum yield oxyfluoride glasses and glass-ceramics

Thomas Meyneng, Jyothis Thomas, Yannick Ledemi, Mathieu Allix, Emmanuel Veron, Cécile Genevois, Raman Kashyap, Younès Messaddeq

► To cite this version:

Thomas Meyneng, Jyothis Thomas, Yannick Ledemi, Mathieu Allix, Emmanuel Veron, et al.. The role of fluorine in high quantum yield oxyfluoride glasses and glass-ceramics. *Journal of Alloys and Compounds*, 2022, 900, pp.163512. 10.1016/j.jallcom.2021.163512 . hal-03611514

HAL Id: hal-03611514

<https://hal.science/hal-03611514>

Submitted on 17 Mar 2022

HAL is a multi-disciplinary open access archive for the deposit and dissemination of scientific research documents, whether they are published or not. The documents may come from teaching and research institutions in France or abroad, or from public or private research centers.

L'archive ouverte pluridisciplinaire **HAL**, est destinée au dépôt et à la diffusion de documents scientifiques de niveau recherche, publiés ou non, émanant des établissements d'enseignement et de recherche français ou étrangers, des laboratoires publics ou privés.

The role of fluorine in high quantum yield oxyfluoride glasses and glass-ceramics

Authors: *Thomas Meyneng¹, Jyothis Thomas², Yannick Ledemi¹, Mathieu Allix³, Emmanuel Veron³, Genevois Cécile³, Raman Kashyap^{2,4}, Younès Messaddeq¹*

1: Laval University, Centre d'Optique et Photonique et Laser

2: Department of Engineering Physics, Polytechnique Montréal

3: CNRS, CEMHTI UPR3079. Orléans, F-45071 Orléans, France

4: Department of Electrical Engineering, Polytechnique Montréal

Corresponding author: Meyneng Thomas,

email : thomas.meyneng.1@ulaval.ca

Phone number (Canada): +1 581 922 1016

Present address : 2375 Rue de la Terrasse, Québec, QC G1V 0A6, Office 2193

Abstract

Oxyfluoride glass-ceramics is considered a great candidate for optical refrigeration. Their ability to form low-phonon fluoride crystals embedded in an oxide glass matrix presents great interest for the development of fluorescent efficient materials with good mechanical and thermal resistance. A better understanding of the material microstructure and its relations on properties is mandatory to achieve the required optical refrigeration values. In the present work, we discuss the effect of fluoride compound evaporations and their impacts on thermal, optical, crystallization, and luminescent properties. Using different melting temperatures, glass samples from the theoretical molar composition $37.6 \text{ SiO}_2 - 22.4 \text{ Al}_2\text{O}_3 - 19 \text{ YF}_3 - 20 \text{ LiF} - 1 \text{ YbF}_3$ are fabricated by the melt-quenching method. The relation between composition and glass properties is assessed by measurement of glass transition, crystallization temperature, density, refractive index, and optical transmission. A detailed study of the crystallization behavior of the samples is conducted using scanning and transmission electron microscopies, and both classical and temperature in-situ x-ray diffractions. Finally, luminescent properties are measured, including quantum yield, and both steady-state and time-resolved spectroscopies.

Keywords: Oxyfluoride, Glass, Transparent glass-ceramics, Ytterbium, Quantum-Yield

1. Introduction

In solids, optical refrigeration is achieved through anti-Stokes fluorescence [1], [2]. Thanks to their well-defined energy levels and low environment sensitivities, lanthanides are one of the chosen candidates. The first optical refrigeration was demonstrated by Epstein et al. in 1995, in a Ytterbium-doped fluoro-zirconate glass, cooled by 0.3 °C from room temperature (300 K) under vacuum [3]. Since then, this cooling phenomenon has been widely deployed either in amorphous or crystalline hosts [4]–[7]. The current record temperature is reported by Melgaard et al. [8] with the cooling of a 10%Yb-doped YLiF₄ single crystal from room temperature (300 K) to 91 K. Single crystals while showing impressive optical performance, are costly and time-consuming to produce. Moreover, their limited geometry constrains their design applications. In contrast, glass-ceramics (GC) is considered an interesting alternative because of their accessible and low-cost productions [9]. Since their discovery in 1993 by Wang and Ohwaki [10], transparent oxyfluoride glass-ceramics (OGCs) are a great compromise between single crystals and amorphous materials. They exhibit a composite nature, with a fluoride crystalline phase embedded in an oxide glass matrix. A low phonon energy environment is provided by the fluoride nature of the crystals [1], which lowers the non-radiative relaxation probability. Consequently, improved fluorescence properties (emission intensity, lifetime, quantum efficiency) are obtained compared to the parent glass or their oxide counterparts [11]–[18]. In this sense, OGCs have been identified as interesting candidates for optical refrigeration purposes [19], [20]. Yttrium fluoride phase glass-ceramics are of particular interest since their performances for laser cooling applications have already been demonstrated as single crystals [5], [8], [21], [22].

Previous work reported the formation of the crystalline phase YLiF₄ (YLF) in the ternary system SiO₂-Al₂O₃-YLiF₄. Deng et al. [15], [23] obtained YLF nanocrystals through the heat treatment of the glass composition 47 SiO₂ – 28 Al₂O₃ – 12 YF₃ – 13 LiF. The authors have reported an increase

in the emission intensity of upconversion fluorescence after ceramization treatment, although no information about the transparency of the samples was given. In 2011, Suzuki [24] obtained similar YLiF_4 -OGCs from the glass composition $43 \text{ SiO}_2 - 23 \text{ Al}_2\text{O}_3 - 17 \text{ YF}_3 - 27 \text{ LiF}$. After a controlled ceramization treatment, the authors reported that the sample transparency was maintained. While these two studies highlight the luminescent potential of these compositions, their analysis in terms of synthesis methods and their impact on material microstructure and properties are not discussed. Herein, we present an optimized composition from the SiO_2 - Al_2O_3 - YLiF_4 system, issued from a previous study [25], and look upon the effect of fluorine concentration on the final glass and glass-ceramic properties. We investigate the effect of the melting parameters, such as temperature and time factors, on the content of fluorine elements in the final composition. Then, using heat treatment at various temperatures, different crystalline phases are obtained. Finally, we discuss the composition effect on both glass and glass-ceramic properties.

2. Material and methods

Three oxyfluoride glass samples with the nominal composition (molar percentages): $37.6 \text{ SiO}_2 - 22.4 \text{ Al}_2\text{O}_3 - 19 \text{ YF}_3 - 20 \text{ LiF} - 1 \text{ YbF}_3$ were prepared using the standard melt-quenching process. The following high purity materials were employed: LiF (5N - AC Materials), YF_3 (5N - AC Materials), YbF_3 (5N - AC Materials), Al_2O_3 (99.997% - Alfa Aesar), and SiO_2 (F300 grade), wet-milled in a zirconia ball planetary miller with UHP water as solvent. The employed ratio was 20g of SiO_2 with 5 mL of water, for 3 cycles of 5 min at 600 RPM, the powder was then dried in a stove for 48 hours. Batches of 8g of glass were prepared for every composition. All the following steps were performed in a dry argon atmosphere glove box. Precursors were mixed in an agate mortar. The mix was then placed in a platinum crucible covered with a lid. Melting was performed in an induction furnace, under a dry argon flow, at different temperature stages for 20 minutes. The temperature is controlled using a thermal camera, adjusted to platinum emissivity, and calibrated for high-

temperature function. The melt was cast in a stainless steel mold pre-heated at 520°C and then annealed at the same temperature for 2h.

The differential scanning calorimetry (DSC) measurements were recorded in a platinum crucible using a Netzsch DSC 404 F3 Pegasus apparatus at a heating rate of 10°C.min⁻¹, from 25 to 1000°C. Glass transition (T_g) and crystallization (T_x) temperatures were determined using the onset method. For (T_g) specifically, we used the first derivative curve to place the onset limits.

The linear refractive index was measured at the wavelengths of 532, 633, 972, 1308 and 1538 nm by using the prism coupling method on a Metricon Mlines 2010.

The density of all samples was obtained via the Archimedes method, using deionized water as immersion liquid, at a temperature of 21°C. The measurement is repeated 10 times and the values are averaged. Errors are calculated from the standard deviation of the 10 values.

UV to Visible transmission data was performed on an Agilent Cary 5000 spectrometer from 200 to 1500 nm and with a Perkin Elmer Frontier FTIR spectrometer from 1,5 to 10 μ m.

Elemental analysis was conducted by electron probe microscopy on a Castaing CAMECA-SX100 apparatus. Wavelength Dispersive Spectroscopy (WDS) was acquired to measure the cationic elements, followed by measurements of fluorine and oxygen using CaF₂ and Al₂O₃ standards, respectively. The presented data is the average value of 8 acquisition measurements. Atomic standard deviation is re-calculated from the weight percent values. To determine the remaining fluorine concentration, normalized the measured concentration by a corrective factor issued from the percentage ratio between measured and theoretical yttrium concentration. In this calculation, we suppose that yttrium evaporation is either negligible or non-existent compared to other elements.

$$x = \frac{f_{\text{exp}}(\text{Yttrium})}{f_{\text{theo}}(\text{Yttrium})}$$

$$[\%F]_{\text{remaining}} = \frac{f_{\text{exp}}(\text{Fluorine})}{x \cdot f_{\text{theo}}(\text{Fluorine})}$$

X-ray powder diffraction data were acquired on an Aeris Panalytical XRD benchtop (Cu $K\alpha_1$ / $K\alpha_2$, radiations). Diffractograms were obtained from 5 to 50° 2 theta, with a step size of 0.011° using 1 second measurements per step. Samples were crushed in an agate mortar and filtered through a 250 microns sieve. Scherrer particle size calculations were performed using reflections 101 and 211 for YLiF₄ (ref 00-017-0874) on 1480-20 samples and 101 and 020 for YF₃ (ref 00-032-1431). In situ, high-temperature X-rays diffraction data were collected using a D8 Advance Bruker Bragg–Brentano diffractometer (Cu $K\alpha_1$ / $K\alpha_2$) equipped with a Vantec-1 linear detector and an HTK1200N Anton Paar oven chamber based on a Kanthal resistive heating attachment. The glass bulk sample was placed on a platinum disk to avoid any reaction with the alumina sample holder and heated from 540°C to 750°C at 30 °C min⁻¹. The temperature behavior and thermal expansion of the setup were previously calibrated using corundum. Isotherm data were collected every 5°C between 15 and 60° (2θ) with a 0.016° step size and a scan total duration of 32 minutes. The Rietveld method was used to quantify the crystalline phase using the TOPAS V6 software 3. The indexed phases refer to the following JCPDS reference : YF₃ (00-068-0059), LiYF₄ (04-005-5663), LiAl(Si₂O₆) (01-073-2336), Y₂Si₂O₅ (00-022-0992), Li₃Al(SiO₅) (01- 084-9301).

Scanning electron microscopy (SEM) images were performed on a FEI Quanta 3D FEG, using 15 kV voltage excitation. Fractures of glass-ceramics were coated with a 10 nm thick Pt/Rh layer to avoid charge effect of the sample.

Transmission electron microscopy (TEM) was used to characterize the nanostructure in glass-ceramic materials. Imaging was performed on a Philips CM20 transmission electron microscope operating at 200kV. A small quantity of sample was crushed with ethanol in an agate mortar. A drop of the suspension was deposited and dried on a copper grid covered by an amorphous holey carbon layer.

Ti: Sapphire laser (Spectra-Physics 3900S, pumped by Millennia 5SJSPG with 5 W) with a pump wavelength of 980 nm were used for collecting the photoluminescence (PL) emission spectra as well as quantum yield (QY) of the samples. The emitted light was collected from an integrating sphere coupled to a multimode optical fiber to an optical spectrum analyzer (OSA) Ando AQ6317B with a working range of 800-1600 nm.

The internal PLQY is defined as the ratio of number of photons emitted to the number of photons absorbed.

$$iQY = \frac{N_{ep} - (1-A)N_{epd}}{N_{ip}A} \quad (1)$$

where N_{ep} is the number of emitted photons from the sample when the sample is inside the integrating sphere and the exciting laser beam is directed onto the sample, N_{ip} is the number of incident photons when the pump laser beam is directed towards empty integrating sphere (without sample), N_{epd} is the number of emitted photons by the sample when the sample is inside the integrating sphere and the exciting laser beam is directed onto the sphere wall (interaction of diffused light).

The Lifetime decay curves obtained upon excitation at 920 nm were acquired with a fast oscilloscope (Tektronix). A photodiode (Thorlabs SM05PD1B) with a resolution of 10 μ s was used to record the signal. The obtained signal was amplified by a benchtop trans-impedance amplifier (Thorlabs PDA200C). Thorlabs MC100A chopper with two slot blades (frequency of 20.0 Hz) was

used to modulate the external signal. In order to block the light at the excitation wavelength, an edge filter was used.

3. Results and discussion.

Glass compositions (molar percent) 37.6 SiO₂ – 22.4 Al₂O₃ – 19 YF₃ – 20 LiF – 1 YbF₃ were prepared at different temperature: 1420 / 1450 / 1480°C for 20 minutes of melting. Atomic elemental analysis of the three glass compositions are reported in table 1 in comparison with the theoretical values.

Table 1. Elemental analysis of the glasses, measured by WDS technique.

	F (At.%)	O (At.%)	Al (At.%)	Si (At.%)	Y (At.%)	Yb (At.%)	Remaining fluorine (%)	Si/F net loss
Theo.	24.63	43.84	13.79	11.58	5.85	0.31		
1420- 20	18.22 (± 0.07)	47.74 (± 0.28)	15.37 (± 0.39)	11.34 (± 0.06)	6.95 (± 0.04)	0.38 (± 0.01)	62	1 : 4.56
1450- 20	17.63 (± 0.5)	48.45 (± 0.37)	15.38 (± 0.36)	11.12 (± 0.12)	7.04 (± 0.07)	0.38 (± 0.01)	59	1 : 4.27
1480- 20	15.59 (± 0.12)	49.79 (± 0.28)	15.72 (± 0.05)	11.36 (± 0.12)	7.16 (± 0.07)	0.38 (± 0.02)	51	1 : 5.17

Analyzing the data reported in Table 1, the concentration of fluorine decreases as the synthesis temperature increases because of evaporation during the melting process. Therefore, the concentration of cationic elements such as aluminum, yttrium, and ytterbium relatively increases with the temperature contrary to the silicon concentration. In fact, it is widely reported that in oxyfluoride glasses synthesis, fluorine compounds evaporation is a common effect [26], [27]. The atomic silicon to fluorine loss ratio appears to be always superior to 4, suggesting that the main evaporation mechanism goes to the formation of gaseous SiF₄ [26]. Additionally, the formation of HF in ambient conditions cannot be excluded. In our case, this process is greatly reduced by the dry melting conditions. Sometimes, the formation of HF can be beneficial as it reacts with adsorbed H₂O

present in the starting materials, which decreases [OH-] groups concentration in the glass melt [28], [29]. Also, LiF evaporation is highly suspected but the quantification of such low atomic mass elements is not reliable.

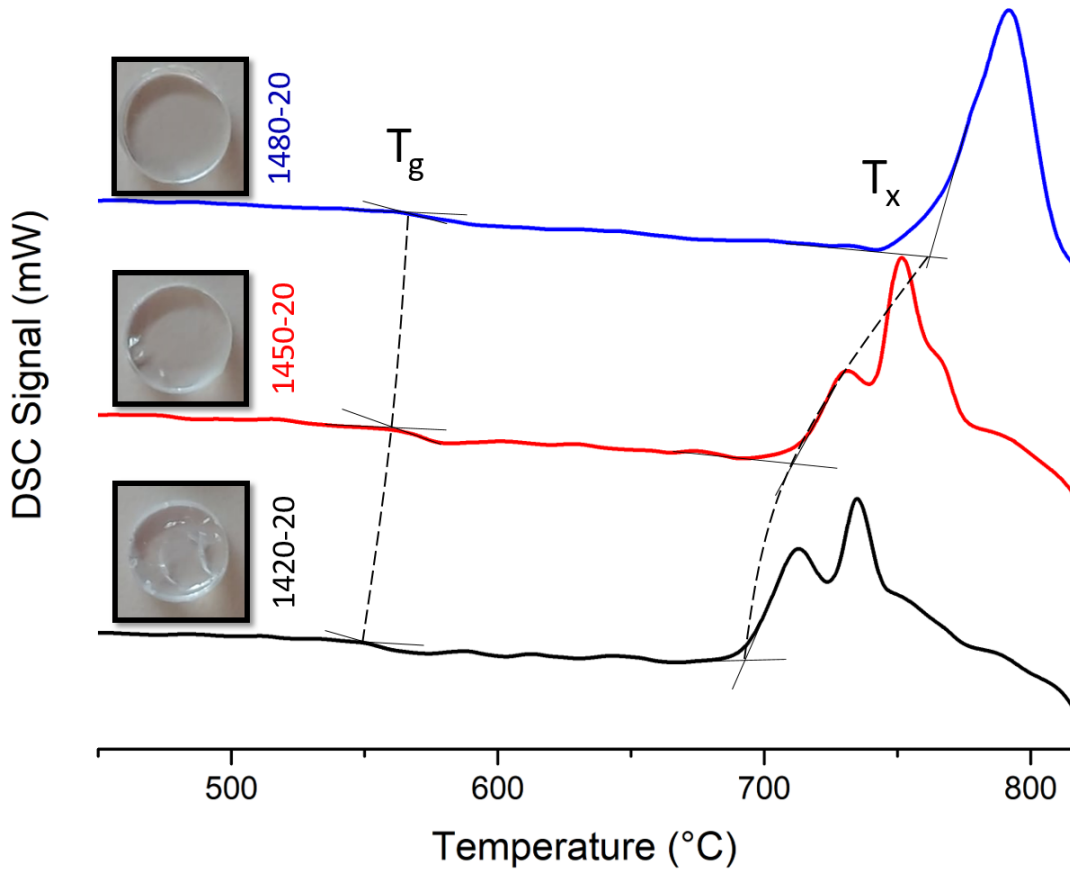


Figure 1. Differential scanning calorimetry curves of the samples were produced at three different melting temperatures. T_g corresponds to the onset of the glass transition temperature and T_x to the onset of the first crystallization observed

Table 2. Onset glass transition temperature(T_g) Crystallization temperature (T_x) and stability parameters of the three glass samples

Sample	T_g ($\pm 2^\circ\text{C}$)	T_x ($\pm 2^\circ\text{C}$)	$\Delta T = (T_x - T_g)$
Glass 1480-20	560	762	202
Glass 1450-20	556	716	160
Glass 1420-20	549	692	143

Figure 1. shows the differential scanning calorimetry (DSC) signal of the three samples. One can observe a slight increase of both glass transition (T_g) and crystallization onset (T_x) and a relative increase of the glass stability parameters defined by ($\Delta T = T_x - T_g$) with lower fluorine concentration (1450-20, 1480-20). In the glass atomic structure, fluorine substitutes oxygen easily given their similar ionic radius. However, fluorine, having a lower degree of oxidation, plays the role of a non-bridging atom, breaking apart the network. Therefore increasing the fluorine concentration has two important effects on glass properties: a lowering of glass-transition temperature (T_g) [30], [31] and a decrease of the viscosity of the glass for a given temperature [32]. Consequently, with the addition of non-bridging entities, both the activation energy for crystallization and the thermal stability of the glass decrease. Interestingly, losses of silica should decrease the network polymerization. This effect is generally linked to a decrease in glass transition temperature [33]–[35]. In our case, this effect does not seem predominant but could participate in limiting glass transition temperature increase with fluorine losses.

Table 3. presents the density value for each of the three glasses. The measured values show a decrease in correlation with higher melting temperature. Since fluorine is a heavier anion compared to oxygen, samples with larger fluorine content present higher density values. Figure 2. shows the refractive index values measured at five different wavelengths by the prism coupling method. Sample 1480-20 presents higher refractive index compared to 1420-20 and 1450-20 samples. Fluorine is an element with low polarizability, lower than oxygen ($\alpha(O) = 0.802 \text{ \AA}^3$; $\alpha(F) = 0.557 \text{ \AA}^3$). Substitution of one element by the other drastically affects the refractive index value and sample density. In fact, a higher amount of fluorine drives to a decrease of the refractive index values, which is the case of the 1420-20 and 1450-20 samples.

Table 3. Density of the glass samples

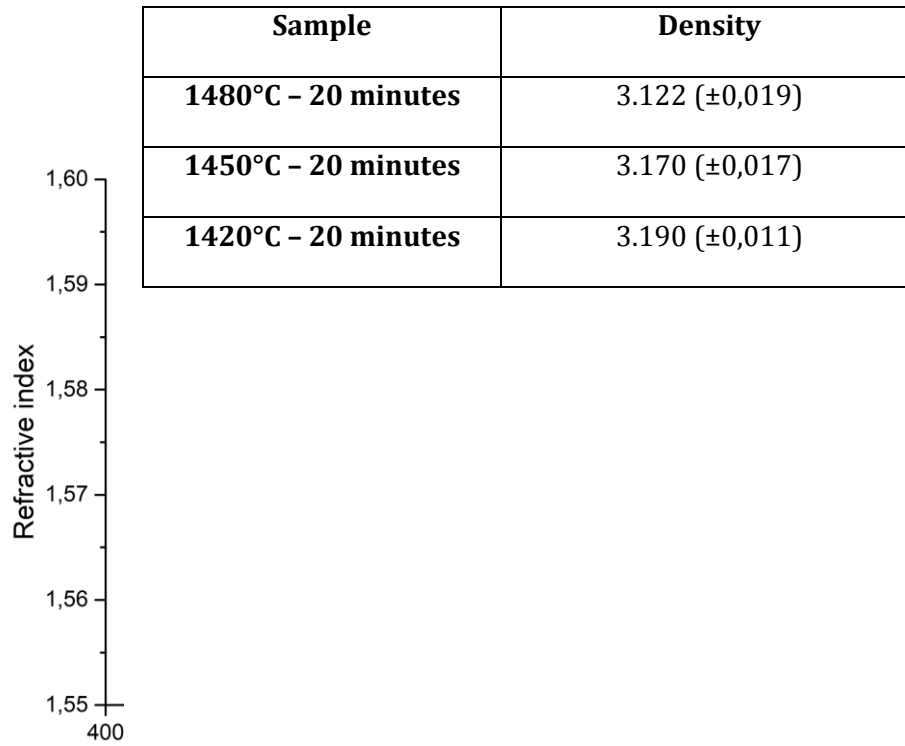


Figure 2. Refractive index of the glasses measured for 5 wavelengths (532, 633, 972, 1308, and 1538 nm)

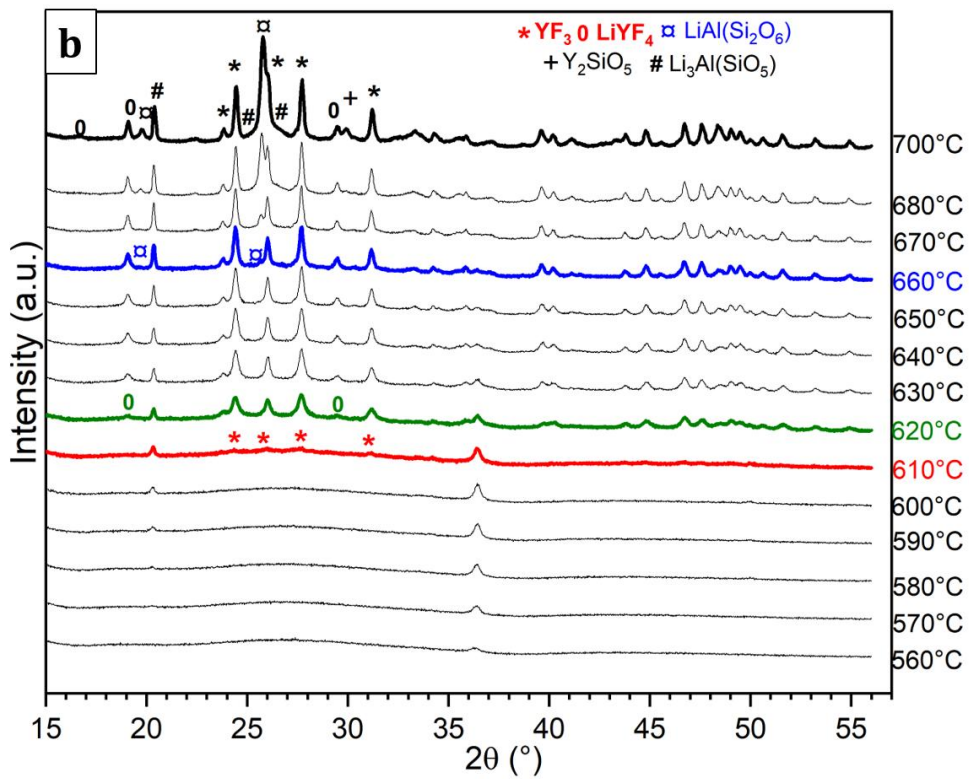
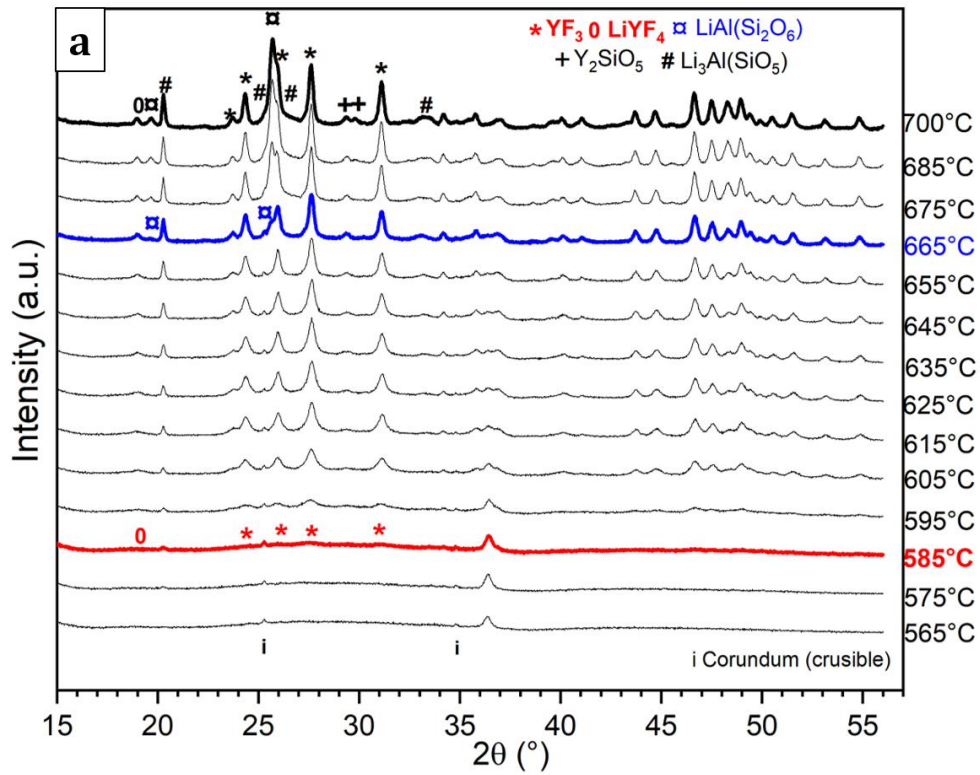


Figure 3. In situ temperature XRD of a. 1480-20 and b. 1420-20 samples

Figure 3. presents in situ high-temperature XRD performed on polished bulk of 1420-20 and 1480-20 samples. The measurement has been performed at temperatures ranging from 540°C to 750°C. For the sample 1420-20, at 585°C, we observe the crystallization at the same time of YF_3 and $LiYF_4$ phases. The large width of the reflection associated with these phases suggests crystallization at the nanometric scale. As the temperature increases, we may note the formation of other crystalline phases such as $Li_3Al(SiO_5)$, $LiAl(Si_2O_6)$, and Y_2SiO_5 . The 1480-20 sample presents a similar crystallization mechanism but shifts at higher temperatures. Indeed, for the glass sample depleted in Fluor, Fluoride phases as YF_3 and $YLiF_4$ appear at 610 and 625°C respectively. As previously observed for the 1420-20 sample, the matrix crystallization takes place at around 660°C with the formation of $LiAl(Si_2O_6)$, followed by $Li_3Al(SiO_5)$ and finally Y_2SiO_5 at 700°C.

The XRD measurements seem to be in good agreement with the DSC analysis presented in figure 1. Samples with higher fluorine content crystallize at lower temperatures ($T_x = 692^\circ\text{C}$ on DSC), attributed to the formation of the YF_3 phase, followed by $YLiF_4$ at the origin of the second exothermic peak. Larger exothermic peaks centered at 750°C were attributed to oxide phase crystallization. However, the sample 1480-20 presents higher onset crystallization ($T_x = 762^\circ\text{C}$) and does not present the clear separation of peaks observed on 1450-20 and 1420-20 samples. This suggests that the crystallization temperature domains are slightly merged.

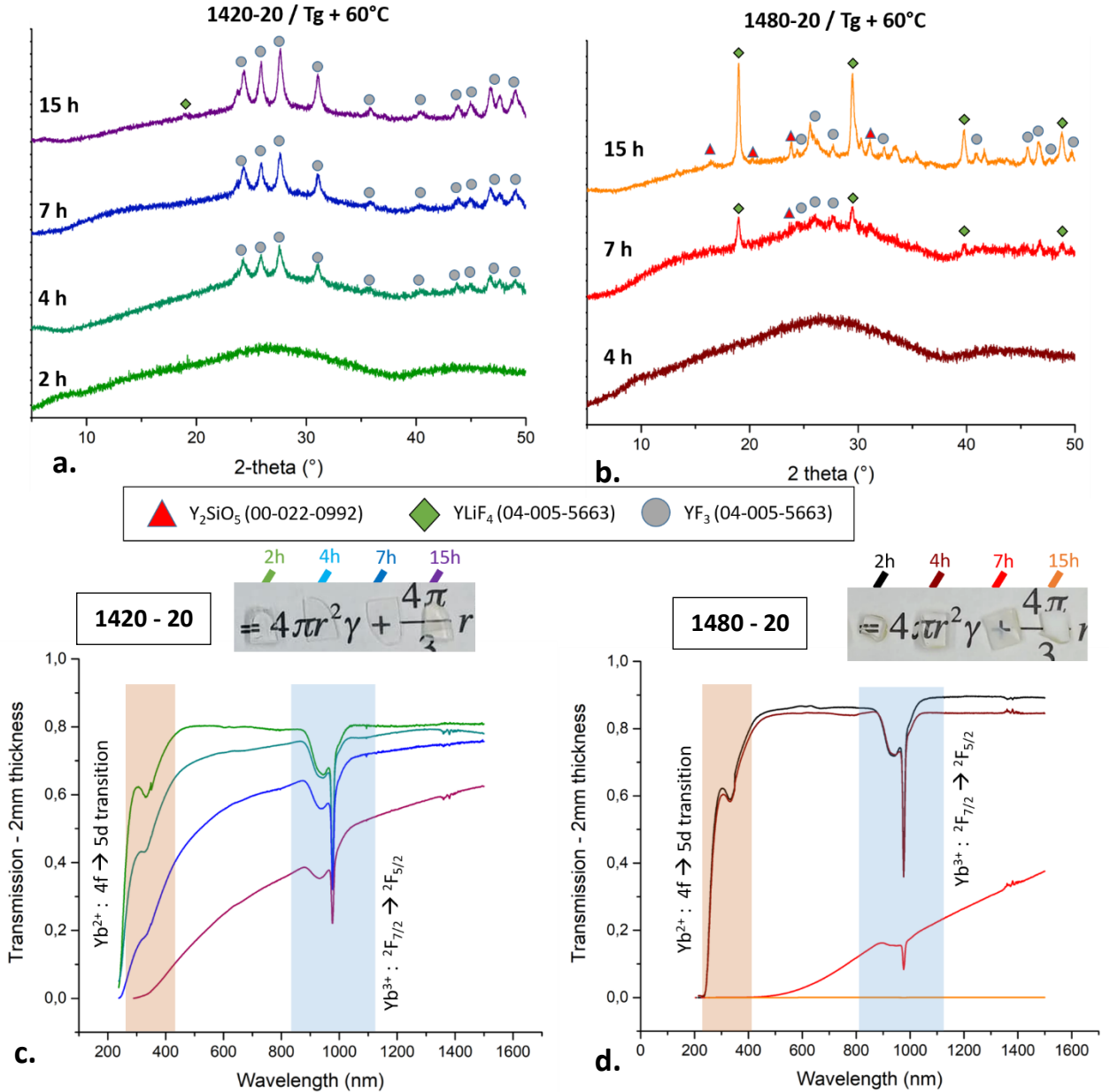


Figure 4. RT X-Ray diffraction of (a) sample 1480-20 treated at T_g+60°C for 4/7/15 h (b) sample 1420-20 treated at T_g+60°C for 2/4/7/15h (c) / (d) transmission values for the treated samples. The blue zone marks the Yb(II) absorption domain, the orange zone corresponds to Yb(III) absorption.

In order to promote the single-phase formation of fluoride crystals, a structural study was performed by heat treatment at T_g+60°C in both samples (1420-20 and 1480-20). Figure 4 (a and b) shows X-ray diffraction data for samples 1420-20 and 1480-20 treated for various duration at T_g+60°C. Figure 4 (c and d) shows transmission measurements performed on the samples 1420-20

and 1480-20 treated at 2/4/7/15h at $T_g+60^\circ\text{C}$. The sample 1420-20 exhibits diffraction peaks after 4 hours of treatment. The angles and intensities of the peaks match with YF_3 . The appearance of diffraction peaks correlates with a wavelength-dependent loss of transmission assigned to Rayleigh scattering arising from the formed crystals. For the sample 1480-20, the main crystalline phase is identified as YLiF_4 with residual peaks of YF_3 and Y_2SiO_5 , after 7 hours of treatment. After 15 hours of heat treatment, the diffraction peaks intensity increases, and the presence of YF_3 and Y_2SiO_5 becomes clearer. The isothermal treatment on the two samples presents different behavior compared to in situ XRD measurements. Mainly, $\text{Li}_3\text{AlSiO}_5$ seems to be absent from those GCs, and most importantly, we were able to obtain GCs with mostly a single crystalline phase. The dynamic nature of temperature in situ XRD explores the crystallization domain of the different phases that can be formed within the current composition/conditions. Isothermal treatment promotes the crystallization of one phase, depending on the chosen temperature. This is the case of the sample 1420-20, for which while increasing the treatment temperature, we obtained a higher fraction of YLiF_4 with the presence of YF_3 as the predominant phase. For 1480-20 samples, the increasing temperature can slightly increase the amount of YF_3 plus the oxide phase. It is important to specify that such conditions of isothermal treatment are appropriate for obtaining GCs with a single predominant phase.

The transmission spectra measurements performed for the two samples show 2 main absorption regions. At 360 nm, near the UV cut-off, the absorption band is related to a $4f \rightarrow 5d$ level transition in Yb (II). The domain from 980 to 1050 nm is related to Ytterbium (III) ${}^2\text{F}_{7/2} \rightarrow {}^2\text{F}_{5/2}$ transition. Similar absorptions were reported by authors in different hosts [36]–[38]. Comparing the transmission spectra of the 2 samples, we observe transmission losses over time due to light scattering in the GCs. The Rayleigh-Gans equation defines the attenuation of a binary system that can be assimilated to a crystal-matrix GCs system with the following equation:

$$\alpha_{RG}(m^2) = \frac{2}{3} N V k^4 r^3 (n\Delta n)^2$$

Where N corresponds to crystallite volumetric density, V the crystallite volume, $k = 2\pi/\lambda$, λ the incident wavelength r the crystallite radius, n the refractive index of the crystallite and Δn the difference of refractive index between the crystallites and the matrix. From this formula, two parameters define a critical effect on the attenuation of light: the radius of the crystals relative to the incident wavelength and the refractive index difference of the crystal/glass system. When optimizing glass-ceramics transparency, the refractive index difference is a parameter to consider when choosing the desired phase and glass system. The second parameter is related to the size of the crystallites which depend on the parameters of heat treatment.

Table 4. Average crystal size diameters calculated from XRD data by Scherrer equation for each treatment time.

	Average crystal diameter (nm)	
	1420-20 / YF3 GCs ± 0.5 nm	1480-20 / YLiF4 GCs ± 0.8 nm
2h	Not detected	Not detected
4h	16	Not detected
7h	18	26
15h	18	33

Table 4 presents crystallite sizes obtained from XRD spectra using the Scherrer equation. Calculated values suggest that crystal sizes in YLiF₄-GCs for the sample 1480-20 are larger than YF₃-GCs present in the 1420-20 sample for similar treatment time. This explains also the difference observed in the transmission spectra. Additionally, YLiF₄-GCs crystallization manifests in an inhomogeneous manner, some parts of the samples are completely transparent while others show high opacification. This could be linked to inhomogeneity of composition in the parent glass, due to the relatively low melting time. This effect was not observed in YF₃-GCs in the 1420-20 sample.

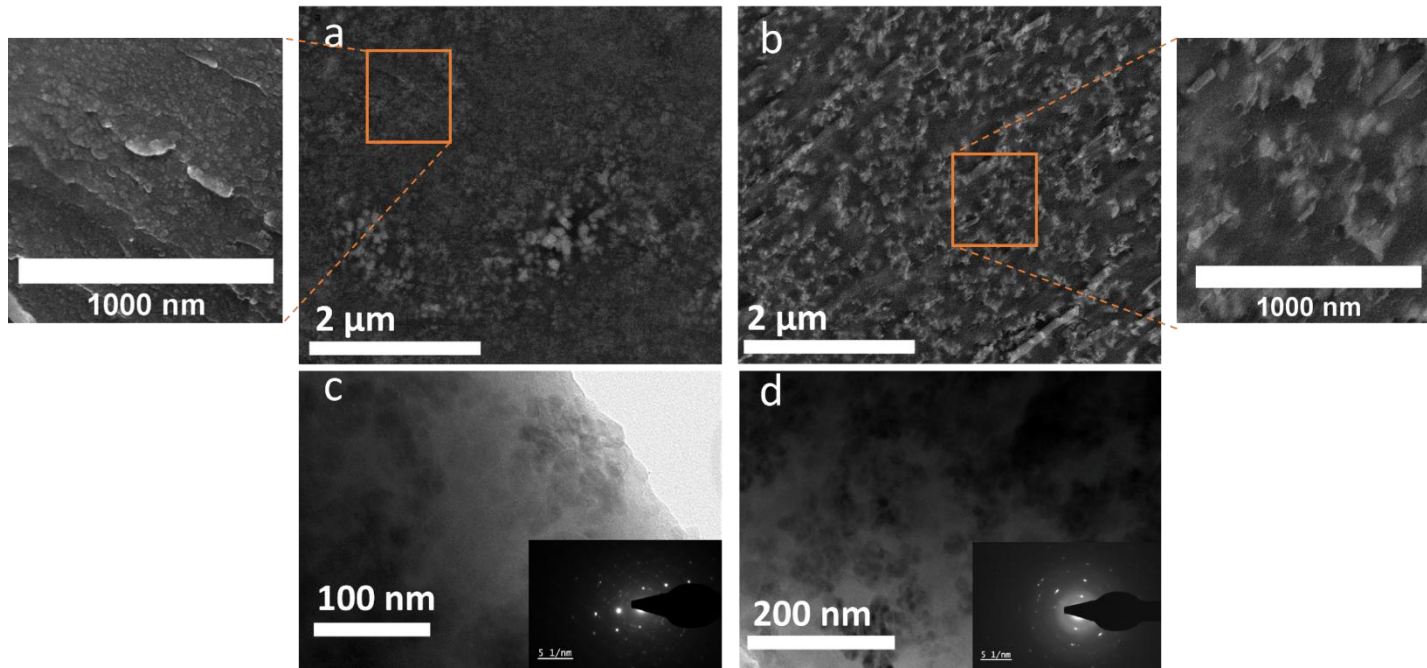


Figure 5. (a,b) Scanning electron microscopy images (backscattering mode) of the glass-ceramics heat-treated for 7-h. (a) corresponds to 1420-20 GCs samples, (b) to 1480-20 GCs samples. Transmission electron microscopy images (bright field mode) of (c) 1420-20 GCs sample and (g) the associated selected area electron diffraction, (d) 1480-20 GCs sample and (h) the associated selected area electron diffraction.

Figure 5 presents pictures of 1420-20 and 1480-20 GCs microstructure after 7h of treatment, obtained through scanning electron microscopy. Backscattering electron acquisition reveals atomic weight contrast, which in our case helps to distinguish fluoride phase crystals apart from the oxyfluoride glass. The 1420-20 GCs show an overall homogeneous and small population of crystals, with the exception of some areas where large crystals (100 to 200 nm) can be identified, suggesting inhomogeneity in the sample. The 1480-20 sample shows crystals with diameters ranging from 20 to 120 nm, an agglomeration effect is also visible, resulting in entities reaching few hundreds of nanometers. We may notice visible inhomogeneity in terms of crystallization, hence some areas appear deprived of any crystals. TEM images reveal a smaller population of crystals in the sample. The average sizes measured are 15.3nm and 13.7nm for the samples 1420-20 and 1480-

20 respectively. The nanoparticles seem to form small agglomerates and the selected area electron diffraction confirms their crystallinity.

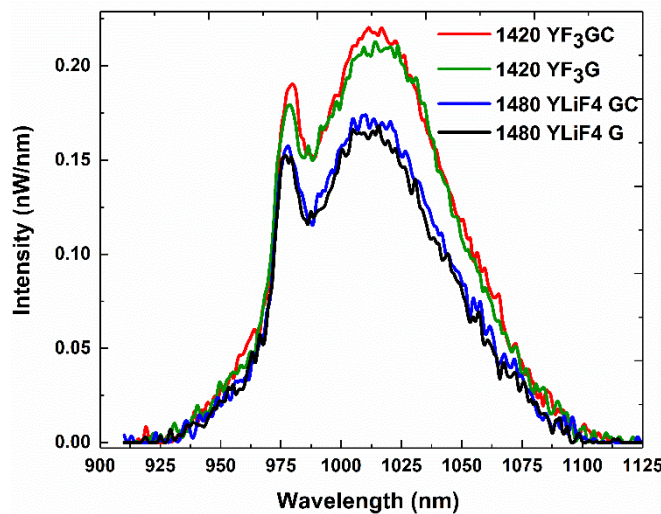


Figure 6. Emission spectra of 1420- YF_3 and 1480- YLiF_4 glass and glass-ceramics samples under 980 nm excitation.

Table 5. Internal Quantum Efficiency (iQY) and lifetime of glass and glass-ceramic samples of 1420-20 and 1480-20 based sample.

Internal Quantum Yield (%) \pm 5%			
Sample	λ_{ex} (nm)	Glass	Glass-Ceramics
YLiF_4 1480-20	920	65%	80%
	980	79%	95%
	1000	70%	79%
YF_3 1420-20	920	67%	84%
	980	83%	96%
	1000	74%	80%
Lifetime (ms) \pm 0.002 ms			
Sample		Glass	Glass-Ceramics
YF_3 1420-20		1.510	1.550
YLiF_4 1480-20		1.410	1.444

The obtained photoluminescence (PL) measurement of glasses and glass-ceramics containing YF_3 and YLiF_4 crystals with 2 mol % of ytterbium at 980 nm is provided in Figure 6. We note that the PL emission intensity of 1420-20 is slightly higher than the intensity of the 1480-20. Table 5 resumes the internal quantum efficiency values (iQY) and lifetime values measured on 1420-20 and 1480-20 samples. We used an integrating sphere method to calculate the iQY and eQY.

The iQY was determined by calculating the ratio of the number of emitted photons to the number of absorbed photons and the eQY by the ratio of the number of emitted photons to the number of exciting laser photons. A detailed procedure can be found in the supplementary information [39]. Maximum iQY is observed at 980 nm excitation. Glass samples of the 1420-20 having a higher amount of fluorine, provide a low-phonon environment for Yb ions, diminishing non-radiative decay. The same tendency is observed through lifetime (LT) measurements, where 1420-20 glass series show longer LT compared to 1480-20 glass samples. Ceramization enhancement effect is observed on both iQY and LT values. We believe this improvement is linked to a change of environment of ytterbium ions, supposedly in a crystalline surrounding, which brings a narrow density of state. The difference in both series is linked to their crystallization behavior. For similar transparency, samples 1480-20 presents a mixture of oxide and fluoride phases which limit the amount of crystalline fraction that can be formed.

4. Conclusion

We report the development of ytterbium-doped glass and glass-ceramics in the $\text{SiO}_2\text{-Al}_2\text{O}_3\text{-YF}_3\text{-LiF}$ system. Three glass samples initiated from the same composition underwent different melting temperatures. Varying time and temperature, we have been able to produce glass-ceramics with the formation of YF_3 or YLiF_4 phase and controlling their transparency. In this paper, we show that by controlling the melting temperature, we have been able to modulate the amount of remaining fluorine in the final glass. Consequently, an interesting compromise can be drawn when choosing between high-fluorine YF_3 GCs and low-fluorine YLiF_4 GCs. The firsts present advantages in terms of fluorescent properties, however, their lower thermal stability towards crystallization could limit their applications as optical fiber. The latter could potentially lead to easier shaping and more diverse design possibilities, not only in laser cooling applications but also in photonic devices. Both YF_3 and YLiF_4 phases are Ytterbium-based crystalline phases, which promote a direct substitution

mechanism when doping with rare-earth, allowing a higher concentration of rare-earth elements and concentration solubility. In order to improve the performance of these materials for optical refrigeration purposes, purification of the glass needs to be incorporated in order to reduce impurities that interfere with ytterbium anti-stokes fluorescence.

Acknowledgment

The authors acknowledge the ICMN laboratory (Orléans, France) for TEM access.

Funding

This work was supported by Laval University and the LIMONCELLO scholarship.

References

- [1] M. P. Hehlen, M. Sheik-Bahae, et R. I. Epstein, « Solid-State Optical Refrigeration », in *Handbook on the Physics and Chemistry of Rare Earths*, vol. 45, Elsevier, 2014, p. 179- 260. doi: 10.1016/B978-0-444-63256-2.00265-5.
- [2] G. Nemova et R. Kashyap, « Laser cooling of solids », *Rep. Prog. Phys.*, vol. 73, n° 8, p. 086501, juill. 2010, doi: 10.1088/0034-4885/73/8/086501.
- [3] R. I. Epstein, M. I. Buchwald, B. C. Edwards, T. R. Gosnell, et C. E. Mungan, « Observation of laser-induced fluorescent cooling of a solid », *Nature*, vol. 377, n° 6549, p. 500- 503, oct. 1995, doi: 10.1038/377500a0.
- [4] J. Fernández, A. Mendioroz, A. J. García, R. Balda, et J. L. Adam, « Anti-Stokes laser-induced internal cooling of Yb³⁺-doped glasses », *Phys. Rev. B*, vol. 62, n° 5, p. 3213- 3217, août 2000, doi: 10.1103/PhysRevB.62.3213.
- [5] S. Bigotta, A. Di Lieto, D. Parisi, A. Toncelli, et M. Tonelli, « Single fluoride crystals as materials for laser cooling applications », San Jose, CA, févr. 2007, p. 64610E. doi: 10.1117/12.701989.
- [6] C. W. Hoyt *et al.*, « Advances in laser cooling of thulium-doped glass », *J. Opt. Soc. Am. B*, vol. 20, n° 5, p. 1066, mai 2003, doi: 10.1364/JOSAB.20.001066.
- [7] B. Zhong, J. Yin, Y. Jia, L. Chen, Y. Hang, et J. Yin, « Laser cooling of Yb³⁺-doped LuLiF₄ crystal », *Opt. Lett.*, vol. 39, n° 9, p. 2747, mai 2014, doi: 10.1364/OL.39.002747.
- [8] S. D. Melgaard, A. R. Albrecht, M. P. Hehlen, et M. Sheik-Bahae, « Solid-state optical refrigeration to sub-100 Kelvin regime », *Sci Rep*, vol. 6, n° 1, p. 20380, avr. 2016, doi: 10.1038/srep20380.
- [9] A. Jha, *Inorganic Glasses for Photonics Fundamentals, Engineering, and Applications*. Chichester, UK: John Wiley & Sons, Ltd, 2016. doi: 10.1002/9781118696088.
- [10] Y. Wang et J. Ohwaki, « New transparent vitroceraamics codoped with Er³⁺ and Yb³⁺ for efficient frequency upconversion », *Appl. Phys. Lett.*, vol. 63, n° 24, p. 3268- 3270, déc. 1993, doi: 10.1063/1.110170.
- [11] P. P. Fedorov, « Transparent oxyfluoride glass ceramics », *Journal of Fluorine Chemistry*, p. 29, 2015.
- [12] A. Tressaud, Éd., *Functionalized inorganic fluorides: synthesis, characterization & properties of nanostructured solids*. Chichester, West Sussex: Wiley, 2010.
- [13] P. P. Fedorov, A. A. Luginina, S. V. Kuznetsov, et V. V. Osiko, « Nanofluorides », *Journal of Fluorine Chemistry*, vol. 132, n° 12, p. 1012- 1039, déc. 2011, doi: 10.1016/j.jfluchem.2011.06.025.
- [14] D. Chen, Y. Wang, Y. Yu, F. Liu, et P. Huang, « Infrared to ultraviolet upconversion luminescence in Nd³⁺ doped nano-glass-ceramic », *Journal of Rare Earths*, vol. 26, n° 3, p. 428- 432, juin 2008, doi: 10.1016/S1002-0721(08)60111-8.
- [15] D. Deng, S. Xu, S. Zhao, C. Li, H. Wang, et H. Ju, « Enhancement of upconversion luminescence in Tm³⁺/Er³⁺/Yb³⁺-codoped glass ceramic containing LiYF₄ nanocrystals », *Journal of Luminescence*, vol. 129, n° 11, p. 1266- 1270, nov. 2009, doi: 10.1016/j.jlumin.2009.06.026.
- [16] Z. Zhao *et al.*, « Er³⁺ Ions-Doped Germano-Gallate Oxyfluoride Glass-Ceramics Containing BaF₂ Nanocrystals », *J. Am. Ceram. Soc.*, vol. 98, n° 7, p. 2117- 2121, juill. 2015, doi: 10.1111/jace.13592.
- [17] J. Heo et C. Liu, « 7 - Fluorescence in Nanostructured Oxyfluoride Glasses Doped with Rare Earth Ions », in *Photonic and Electronic Properties of Fluoride Materials*, A. Tressaud et K. Poeppelmeier, Éd. Boston: Elsevier, 2016, p. 139- 157. doi: 10.1016/B978-0-12-801639-8.00007-6.
- [18] Y. Ledemi *et al.*, « White light and multicolor emission tuning in triply doped Yb³⁺ /Tm³⁺ /Er³⁺ novel fluoro-phosphate transparent glass-ceramics », *J. Mater. Chem. C*, vol. 2, n° 25, p. 5046- 5056, 2014, doi: 10.1039/C4TC00455H.

- [19] G. Nemova et R. Kashyap, « Laser cooling with Tm³⁺-doped oxy-fluoride glass ceramic », *J. Opt. Soc. Am. B, JOSAB*, vol. 29, n° 11, p. 3034- 3038, nov. 2012, doi: 10.1364/JOSAB.29.003034.
- [20] J. Thomas *et al.*, « Oxyfluoride glass-ceramics: a bright future for laser cooling », in *Photonic Heat Engines: Science and Applications II*, févr. 2020, vol. 11298, p. 112980E. doi: 10.1117/12.2546969.
- [21] D. Seletskiy, M. P. Hasselbeck, M. Sheik-Bahae, R. I. Epstein, S. Bigotta, et M. Tonelli, « Cooling of Yb:YLF using cavity enhanced resonant absorption », San Jose, CA, févr. 2008, p. 69070B. doi: 10.1117/12.759152.
- [22] S. Melgaard, D. Seletskiy, A. Albrecht, et M. Sheik-Bahae, « First solid-state cooling below 100K », *SPIE Newsroom*, mars 2015, doi: 10.1117/2.1201503.005790.
- [23] D. Deng *et al.*, « Blue cooperative upconversion in Yb³⁺-doped glass ceramic containing LiYF₄ nanocrystals », *J. Phys. D: Appl. Phys.*, vol. 42, n° 10, p. 105111, mai 2009, doi: 10.1088/0022-3727/42/10/105111.
- [24] T. Suzuki, S. Masaki, K. Mizuno, S. Mizuno, et Y. Ohishi, « Synthesis of novel transparent glass-ceramics containing rare earth ion-doped YLF nanocrystals for fiber amplifiers and fiber lasers », San Francisco, California, févr. 2011, p. 793403. doi: 10.1117/12.874309.
- [25] J. Thomas *et al.*, « Enhanced anti-Stokes emission in oxyfluoride glass ceramics for optical refrigeration », in *Photonic Heat Engines: Science and Applications III*, Online Only, United States, mars 2021, p. 20. doi: 10.1117/12.2582809.
- [26] K. Shimizu, « Fluoride Evaporation from CaF₂-SiO₂-CaO Slags and Mold Fluxes in Dry and Humid Atmospheres », *High Temperature Materials and Processes*, vol. 22, p. 10, 2003.
- [27] D. Möncke *et al.*, « NaPO₃-AlF₃ GLASSES: FLUORINE EVAPORATION DURING MELTING AND THE RESULTING VARIATIONS IN STRUCTURE AND PROPERTIES », p. 15, 2018.
- [28] R. Zheng *et al.*, « Novel Synthesis of Low Hydroxyl Content Yb³⁺-Doped Fluorophosphate Glasses with Long Fluorescence Lifetimes », *J. Am. Ceram. Soc.*, vol. 98, n° 3, p. 861- 866, mars 2015, doi: 10.1111/jace.13386.
- [29] S. Xu, P. Wang, R. Zheng, W. Wei, et B. Peng, « Effects of alkaline-earth fluorides and OH⁻ on spectroscopic properties of Yb³⁺ doped TeO₂-ZnO-B₂O₃ based glasses », *Journal of Luminescence*, vol. 140, p. 26- 29, août 2013, doi: 10.1016/j.jlumin.2013.02.056.
- [30] M. Reben et M. Środa, « Influence of fluorine on thermal properties of lead oxyfluoride glass », *J Therm Anal Calorim*, vol. 113, n° 1, p. 77- 81, juill. 2013, doi: 10.1007/s10973-013-3047-x.
- [31] M. Środa, « Effect of LaF₃ admixture on thermal stability of borosilicate glasses », *J Therm Anal Calorim*, vol. 88, n° 1, p. 245- 249, avr. 2007, doi: 10.1007/s10973-006-8137-6.
- [32] J. Kirchhof, S. Unger, et J. Dellith, « Viscosity of fluorine-doped silica glasses », *Opt. Mater. Express*, vol. 8, n° 9, p. 2559, sept. 2018, doi: 10.1364/OME.8.002559.
- [33] M. Ciecńska, P. Goj, A. Stoch, et P. Stoch, « Thermal properties of 60P2O₅-(40-x)Al₂O₃-xNa₂O glasses », *J Therm Anal Calorim*, vol. 139, n° 3, p. 1763- 1769, févr. 2020, doi: 10.1007/s10973-019-08606-w.
- [34] I. Ben Kacem, L. Gautron, D. Coillot, et D. R. Neuville, « Structure and properties of lead silicate glasses and melts », *Chemical Geology*, vol. 461, p. 104- 114, juin 2017, doi: 10.1016/j.chemgeo.2017.03.030.
- [35] J. Zarzycki, *Glasses and the vitreous state*. Cambridge : New York: Cambridge University Press, 1991.
- [36] M. Henke, J. Perßon, et S. Kück, « Preparation and spectroscopy of Yb²⁺-doped Y₃Al₅O₁₂, YAlO₃, and LiBaF₃ », *Journal of Luminescence*, vol. 87- 89, p. 1049- 1051, mai 2000, doi: 10.1016/S0022-2313(99)00535-9.
- [37] M. Engholm, L. Norin, et D. Åberg, « Strong UV absorption and visible luminescence in ytterbium-doped aluminosilicate glass under UV excitation », *Opt. Lett.*, vol. 32, n° 22, p. 3352, nov. 2007, doi: 10.1364/OL.32.003352.

- [38] C. Xia, G. Zhou, Y. Han, X. Zhao, et L. Hou, « Luminescence of Yb²⁺, Yb³⁺ co-doped silica glass for white light source », *Optical Materials*, vol. 34, n° 5, p. 769- 771, mars 2012, doi: 10.1016/j.optmat.2011.11.002.
- [39] E. S. de L. Filho *et al.*, « Ytterbium-doped glass-ceramics for optical refrigeration », *Opt. Express, OE*, vol. 23, n° 4, p. 4630- 4640, févr. 2015, doi: 10.1364/OE.23.004630.